Near-Infrared Excitation of the *Q* Band in Free Base and Zinc Tetratolyl-porphyrins

Oliver Schalk,[†] Helge Brands,[†] Teodor Silviu Balaban,[‡] and Andreas-Neil Unterreiner*[,†]

Karlsruhe Institute of Technology, Institute for Physical Chemistry and Center for Functional Nanostructures, University of Karlsruhe (TH), D-76128 Karlsruhe, Germany, and Karlsruhe Institute of Technology, Forschungszentrum Karlsruhe, Institute for Nanotechnology and Center for Functional Nanostructures, University of Karlsruhe (TH), D-76021 Karlsruhe, Germany

Received: July 26, 2007; In Final Form: November 15, 2007

The photophysics of 5,10,15,20-tetra-*p*-tolyl-21*H*,23*H*-porphyrin (TTP−H_2) and 5,10,15,20-tetra-*p*-tolyl-porphyrinato zinc II (ZnTTP) have been investigated by means of pump−probe and transient anisotropy experiments. After excitation to the *Q* band, the molecules were probed by NIR pulses in the range between 950 and 1350 nm in order to study states of gerade symmetry in the vicinity of the Soret band. Examination of transient spectra and anisotropy delivered the first direct observation and the excitation energies of the two lowest so-called dark states. The experimental results were compared with predictions from theoretical calculations.

1. Introduction

Porphyrins, metalloporphyrins, and their related compounds are of great scientific and industrial interest. Iron-containing porphyrins are found in hemoproteins, for example, hemoglobin and myoglobin, which are responsible for oxygen transfer in blood.[1] Tetrapyrrolic macrocycla related to the porphyrins can also be found in chlorophylls, which are magnesium-chlorins, that is, porphyrins where one of the four pyrrol subunits is reduced to a pyrroline. Chlorophylls serve mainly as light harvesting complexes in plants and photosynthetic bacteria.[1] Synthetic porphyrin derivatives are promising candidates as antenna molecules in solar cells,[2−4] elements in molecular logic circuits,[5,6] or effective sensitizers in anticancer treatments as photodynamic (PDT), photothermic (PTT), or boron neutron capture therapies (BNCT).[7−11] In most applications, the porphyrin derivatives serve as light-harvesting molecules. Therefore, a thorough understanding of its photophysical and photochemical processes are of fundamental interest.

Consequently, various studies have been dedicated to this field,[12−14] especially to characterize absorption and fluorescence spectra[15−32] and to study ultrafast dynamics after photoexcitation.[32−57] The absorption spectra of porphyrins exhibit several characteristic bands.[12,13] The transition to the lowest-energy excited singlet state (often referred to as S_1 state) is called the *Q* band. In the case of molecules with D_{4h} symmetry, it has ^1E_u symmetry. There are two or three peaks between 500 and 650 nm separated by ≈1250 cm^{-1}. The different peaks, denoted as *Q*(0,0), *Q*(1,0), and so forth, can be assigned to several different vibronic states. In the case of a lower symmetry, for example, D_{2h} in free base porphyrins, this band is further split into the Q_x and the Q_y bands, where the Q_x band has a lower excitation energy and extinction coefficient (see Figure 1 for the stationary absorption spectrum of 5,10,15,20-tetra-*p*-tolyl-21*H*,23*H*-porphyrine (TTP−H_2) in dichlormethane and 5,10,15,20-tetra-*p*-tolyl-porphyrinato zinc II (ZnTTP) in cyclohexane). The transition to the S_2 state is called *B* or Soret band and has the same symmetry as the *Q* band but a much higher extinction coefficient. In solution, it peaks between 400 and 420 nm with a shoulder on its blue side probably due to vibrational progression.[32,33] The Soret band is energetically not split in porphyrins with lower symmetry, however a bright absorbing state near the Soret band has recently been discussed.[31−33]

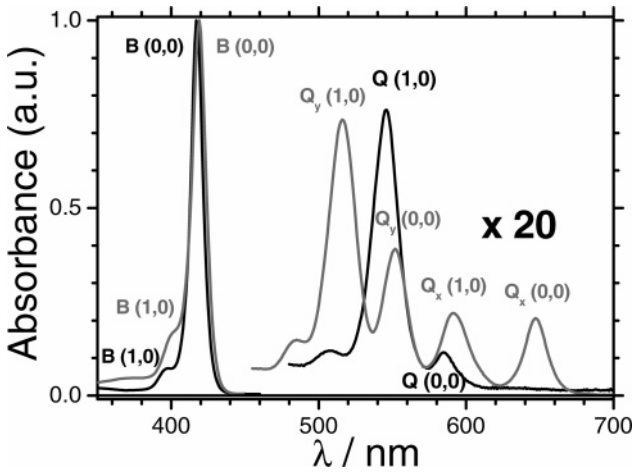

Figure 1. UV−vis spectra of ZnTTP in cyclohexane (black) and TTP−H_2 in dichloromethane (gray). The spectrum is multiplied by a factor 20 for $\lambda > 480$ nm.

Q and *B* bands can be explained by simple models such as the "particle on a ring" model[58,59] or the four-orbital model;[15,16] however, these models do not predict the existence of dark states in the Soret region, that is, states with gerade symmetry that cannot be seen due to the $u-g$ selection rule. The existence of these states has been discussed on the basis of quantum chemical calculations[30,60] and was used to explain the relaxation dynamics following the *B* band excitation.[32] This also plays an important role in the interpretation of previous experiments, where the dark states serve as pathways for fast energy dissipation. However, these states have not been excited directly in an experiment before, therefore, the exact location of these states is still unknown. One possibility to probe these states are experiments with femtosecond time resolution. In the following,

* Corresponding author. E-mail: andreas.unterreiner@kit.edu.
[†] Institute for Physical Chemistry.
[‡] Institute for Nanotechnology.

10.1021/jp075907z CCC: $40.75
Published on Web 02/06/2008

we will present pump−probe and transient anisotropy measurements where we excited the $Q_x(0,0)$, $Q_y(0,0)$, and $Q_y(1,0)$ transitions of TTP−H_2 in dichloromethane and the $Q(1,0)$ transition of ZnTTP in cyclohexane and probed with NIR pulses in the range between 950 and 1350 nm. In doing so, the region near the Soret band is scanned while potential triplet excitations are avoided that might occur after intersystem crossing (ISC).[12] Since excitation to the *Q* band promotes the porphyrin to an ungerade state, the NIR pulse is sensitive for the gerade or dark states.

2. Experimental Section

Materials. ZnTTP was prepared by the Rothemund condensation of para-tolualdehyde with pyrrole in the presence of zinc acetate in refluxing collidine.[61] Column chromatography on silica gel with dichloromethane provided pure ZnTTP, free of any chlorin which can accompany commercial batches of this product that is usually prepared by the Adler-Longo synthesis in refluxing propionic acid.[62]

Zinc demetallation to the free base (TTP−H_2) was performed on a 100 mg scale by stirring ZnTTP for 1 h under argon at room temperature with a mixture of 10 mL trifluoroacetic acid and 5 mL sulfuric acid 98%. After pouring on crushed ice, extraction into dichloromethane and washing until neutral with sodium hydrogen carbonate and with brine, the residue was chromatographed on a silica gel column eluted with freshly distilled dichloromethane.

The sample purities were checked by NMR (Bruker) and MALDI-ToF mass spectrometry (Applied Biosystems). Solvents were thoroughly dried as follows: cyclohexane was refluxed overnight from sodium metal and distilled prior to use; dichloromethane was refluxed over calcium hydride and distilled freshly before use.

Experimental Setup. Time-resolved pump−probe absorption spectroscopy and transient anisotropy were used to investigate the ultrafast dynamics of ZnTTP in cyclohexane and TTP−H_2 in dichloromethane. The tolyl-porphyrins were used instead of the commonly studied phenyl derivatives because of two reasons; (i) the tolyl derivatives have a higher purity compared with the phenyl derivatives because of the preparation process (no chlorins, see above), and (ii) the zinc tolyl derivative can be better solved in nonpolar solvents such as cyclohexane, which exhibit only a weak solvent−solute interaction. The samples were prepared in a cuvette (Hellma QS) with an optical path length of 1 mm. The optical density at the pump wavelength was typically 0.05 for ZnTTP and between 0.05 for the $Q_x(0,0)$ and 0.2 for the $Q_y(0,1)$ band of TTP−H_2. A typical ΔOD value of 0.002 in the transients, therefore, signifies that ≤5% of the excited molecules are probed. Both pump and probe pulses were derived from two NOPAs (noncollinear optical parametric amplifier[63,64]) tunable from 470 to 1600 nm that were pumped by a commercial 1 kHz amplified femtosecond Ti:sapphire laser system (Clark-MXR, CPA 2210). Although the phosphorescence lifetime of, for example, TPP−H_2 in EPA (ethyl ether/isopentane/ethanol in a volume ratio of 5:5:2) is $\tau_p = 6.6$ ms and therewith exceeds the repetition rate of the laser setup, the triplet yield is only 2×10^{-5};[65] therefore, a negligible part of the molecules is not in its ground state. The pulse duration was about 80 fs, and the spectral width was approximately 40 nm for the visible pump−pulses and 50 nm for the NIR pulses depending slightly on the wavelength. Because of this width, the probe wavelength was varied in steps of 50 nm. Note that the spectral width in the visible is small enough to ensure the excitation of the desired porphyrin bands exclusively (see the spectra in Figure 1). The temporal resolution of the experiment was ∼130 fs since group velocity mismatch in the sample could not be avoided. Note that samples which are too concentrated can exhibit remarkable aggregation effects.[1] In our experiments, we optimized toward transient amplitudes and not to time resolution. The pump−pulse was mechanically chopped and temporally delayed relative to the probe pulses using a computer controlled translation stage (Physik Instrumente). The pump−pulse energy at various wavelengths was varied between 0.4 and 2 μJ/pulse in order to check the energy dependence of the signal. Since no such dependence could be detected, experiments were performed at a pump energy of 1.6 μJ/pulse. The probe pulse energy was less than 10 nJ/pulse. The probe beam diameter was smaller than half of the pump beam, which was about 2 mm. Reference measurements in pure solvents without porphyrins gave no significant ΔOD amplitudes under these conditions. Both laser beams were slightly focused. The polarization of the probe beam was set either at 45° or at magic angle (≈54.7°) with respect to the pump beam by means of a tunable λ/2 plate (Alphalas). Intensities of the probe pulse before and behind the sample cell were detected by InGaAs photodiodes (Hamamatsu) and the change of the optical density with and without pump−pulse, Δ*OD*, was recorded. In anisotropy measurements, a Glan-Taylor polarizer (Alphalas) was used to simultaneously monitor the change of the optical density for the parallel ($\Delta OD_{\parallel}$) and perpendicular ($\Delta OD_{\perp}$) components. The anisotropy $r(t)$ value can be calculated thereafter by:[66,67]

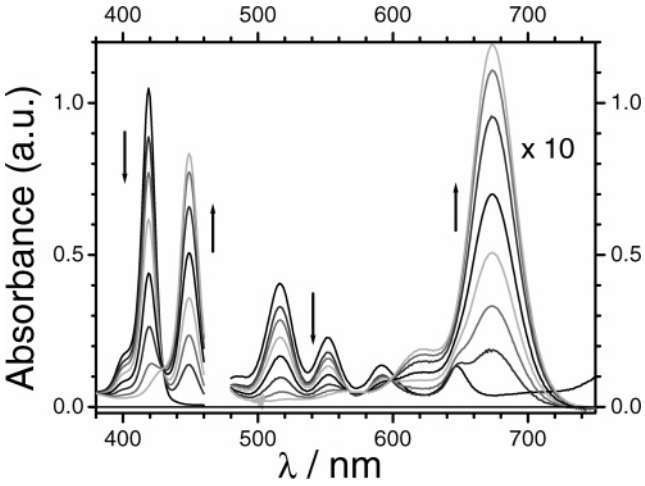

Figure 2. UV−vis spectra of TTP−H_2 in dichloromethane after different irradiation times with a xenon arc lamp; the arrows denote the temporal evolution. The spectum is multiplied by a factor of 10 for $\lambda > 480$ nm.

$$r(t) = \frac{\Delta OD_{\parallel}(t) - \Delta OD_{\perp}(t)}{\Delta OD_{\parallel}(t) + 2 \cdot \Delta OD_{\perp}(t)} \qquad (1)$$

Some details of the evaluation of anisotropy data are given in Appendix A. The anisotropy was checked by sulforhodamine B in ethanol, which is supposed to give a time zero anisotropy of $r_0 = 0.37$.[68] Since porphyrins dissolved in dichloromethane are known to exhibit a charge transfer to solvent (CTTS) transition followed by a reaction with the solvent or residual water,[33,69,70] the sample was exchanged after each experiment, although no difference in the transients was detected. In order to study a possible influence of the CTTS product, irradiation measurements with a xenon arc lamp (Ushio Inc.) were performed. A typical measurement can be seen in Figure 2. Obviously, when exciting the Q_y band, the product shows no

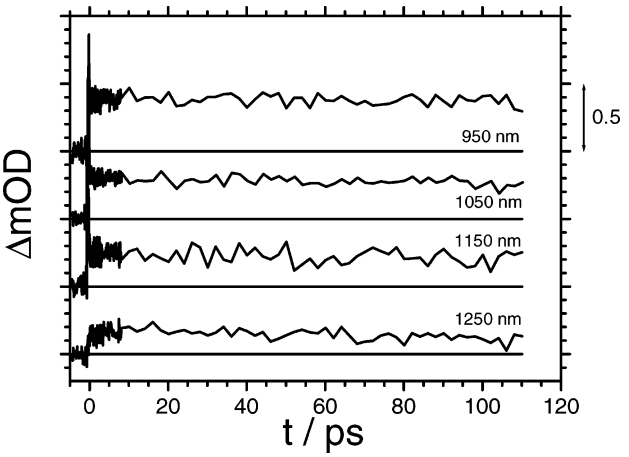

Figure 3. Transients of TTP−H_2 after excitation with 647 nm (shifted for clarity).

absorption in this region, so the pump−pulse only excites the porphyrin. However, when exciting the Q_x band, care has to be taken. Note that the reaction also occurred when the sample was irradiated with $\lambda > 500$ nm using a high-pass filter (Schott, OG 515) in front of the arc lamp. A detailed analysis will soon be published.

3. Results

3.1. Steady State Measurements. UV−vis spectra (Varian, Cary 5E) for TTP−H_2 in dichloromethane (gray curve) and Zn-TTP in cyclohexane (black curve) are shown in Figure 1. Maxima are found at 419 nm for the *B* band and at 485, 516, 552, 592, and 647 nm for the $Q_y(2,0)$, $Q_y(1,0)$, $Q_y(0,0)$, $Q_x(1,0)$, and $Q_x(0,0)$ transition of TTP−H_2, respectively. For ZnTTP, the *B* band peaks at 417 nm and 506, 546, and 584 nm for the *Q* band, respectively. The TTP−H_2 peaks agree well with the spectrum of free base tetraphenyl-porphyrin (TPP−H_2) dissolved in chloroform[23] while the ZnTTP spectrum is red-shifted by approximately 2 nm compared with zinc(II)-tetraphenyl-porphyrin (ZnTPP) in hexane.[32]

Fluorescence spectra upon excitation at 550 nm (Cary Eclipse fluorimeter) were measured in 1 cm cuvettes (Hellma). The spectra were corrected and peaked at 596 and 646 nm for ZnTTP and at 653 and 718 nm for TTP−H_2.

3.2. Pump−Probe and Transient Anisotropy Experiments. *3.2.1. Tetratolylporphyrin.* Pump−probe and transient anisotropy measurements of tetratolylporphyrin in dichlormethane have been performed by varying both pump and probe wavelengths.

Excitation to the Q_x State: Figure 3 shows the pump−probe transients after excitation to the $Q_x(0,0)$ band at 647 nm. The probe wavelength was varied between 950 and 1250 nm. At wavelengths beyond 1250 nm, the transients were too weak for a thorough analysis. The transients exhibit no dynamics on a femtosecond time scale but on a time scale ≫100 ps independent of the probe wavelength as found for the S_1-T_1 transition in earlier investigations of TPP−H_2.[34,71,72] In Figure 4c, a transient spectrum collected from the different pump−probe measurements can be seen. The black curve is the normalized steady-state spectrum of TTP−H_2 while the symbols represent the normalized ΔOD values of various probe wavelengths after 200 fs (black squares), 500 fs (dark circles), 1 ps (gray triangles), and 20 ps (pale reversed triangles). The spectra are nearly identical for all delay times. Various symbols represent the total energy of pump and probe photons. In Figure 5, raw, that is, non-deconvoluted anisotropy profiles, are shown for different probe wavelengths following 647 nm excitation. The time zero anisotropy decreases with increasing probe wavelength. A biexponential behavior can be found with time constants of $\tau_1^a = 350-700$ fs and $\tau_2^a \gg 100$ ps where the latter can be assigned to rotational diffusion. The explicit values can be found in Table 1.

Excitation to the Q_y State: Excitation of the $Q_y(0,0)$ and the $Q_y(1,0)$ states was performed at pump wavelengths of 514 and 546 nm, respectively. The probe wavelength was varied between 950 and 1250 nm (1350 nm for $\lambda_{pump} = 546$ nm). Figure 6 shows several transients for an excitation wavelength of 514 nm. Each transient can be fitted with a triexponential decay where $\tau_1 = (170 \pm 30)$ fs, $\tau_2 = (1200 \pm 300)$ fs and $\tau_3 \gg 300$ ps independent of the probe wavelength except for 1100 nm, where $\tau_2 = (2000 \pm 200)$ fs. One main feature is the difference in the amplitudes A_2 and A_3 for τ_2 and τ_3. Let the relative weight be defined as

$$w(A_i) = \frac{A_i}{A_2 + A_3} \qquad \text{where } i = 2, 3 \tag{2}$$

While at 1000 and 1250 nm, $w(A_2)$ is nearly 30%, it decreases to a value of below 10% for a probe wavelength of 1100 nm. Transient spectra can be seen in Figure 4a. As in Figure 4c, the steady-state spectrum in the Soret region is compared with the energy of the ground state of the Q_x band and the probe pulse. One sees a distinct maximum at a probe wavelength of 1050 nm.

Similar results are obtained when pumping the $Q_y(0,0)$ state at 546 nm. Here, the transients can be well-fitted by a biexponential decay with time constants τ_2 and τ_3. The first time constant, τ_1, is supposed to be faster than the time resolution (see discussion). The corresponding transient spectrum can be seen in Figure 4b peaking at 1050 nm. All fitted parameters can be found in Tables 1 and 2.

Selected anisotropy measurements at a pump wavelength of 514 nm are shown in Figure 7. They exhibit a fast rise, a maximum at $\tau \approx 200$ fs and a fast decay to a value r_s, being constant on a 10 ps time scale. Finally, the anisotropy decays with a time constant of approximately 150−200 ps. The time zero anisotropy as well as r_s become smaller with increasing probe wavelengths. At $\lambda_{probe} = 1250$ nm, no intermediate maximum of the anisotropy can be seen.

Anisotropy measurements with a pump wavelength of $\lambda_{pump} = 546$ nm (not shown) also exhibit no maximum in the probed range between 950 and 1150 nm; the monoexponential decay on the short time scale is faster than for $\lambda_{pump} = 647$ nm, while a second decay constant is on the order of 150−200 ps as for $\lambda_{pump} = 514$ nm. At longer probe wavelengths, a maximum can be seen.

3.2.2. Zinc-tetratolylporphyrin. Pump−probe and transient anisotropy measurements have been performed by a single pump wavelength of 546 nm ($Q(1,0)$ transition) because of the small oscillator strength of the other *Q* absorption peaks. The probe wavelength was varied between 950 and 1350 nm. Selected measurements can be seen in Figure 8. The pump−probe transients can be modeled by a two-exponential decay (see Table 3). Between 1350 and 1100 nm, the time constants were wavelength independent ($\tau_1 = (1300 \pm 300)$ fs and $\tau_2 \gg 500$ ps), while at larger wavelengths, τ_1 gradually increases up to (4.9 ± 0.5) ps at 950 nm. The fitting convergence of the transients is not significantly improved when using a triexponential decay. The spectra shown in Figure 4d are analogous to the spectra for TTP−H_2. Here, the energy for the transient spectra are the sum of the $Q(0,0)$ transition at 584 nm and the

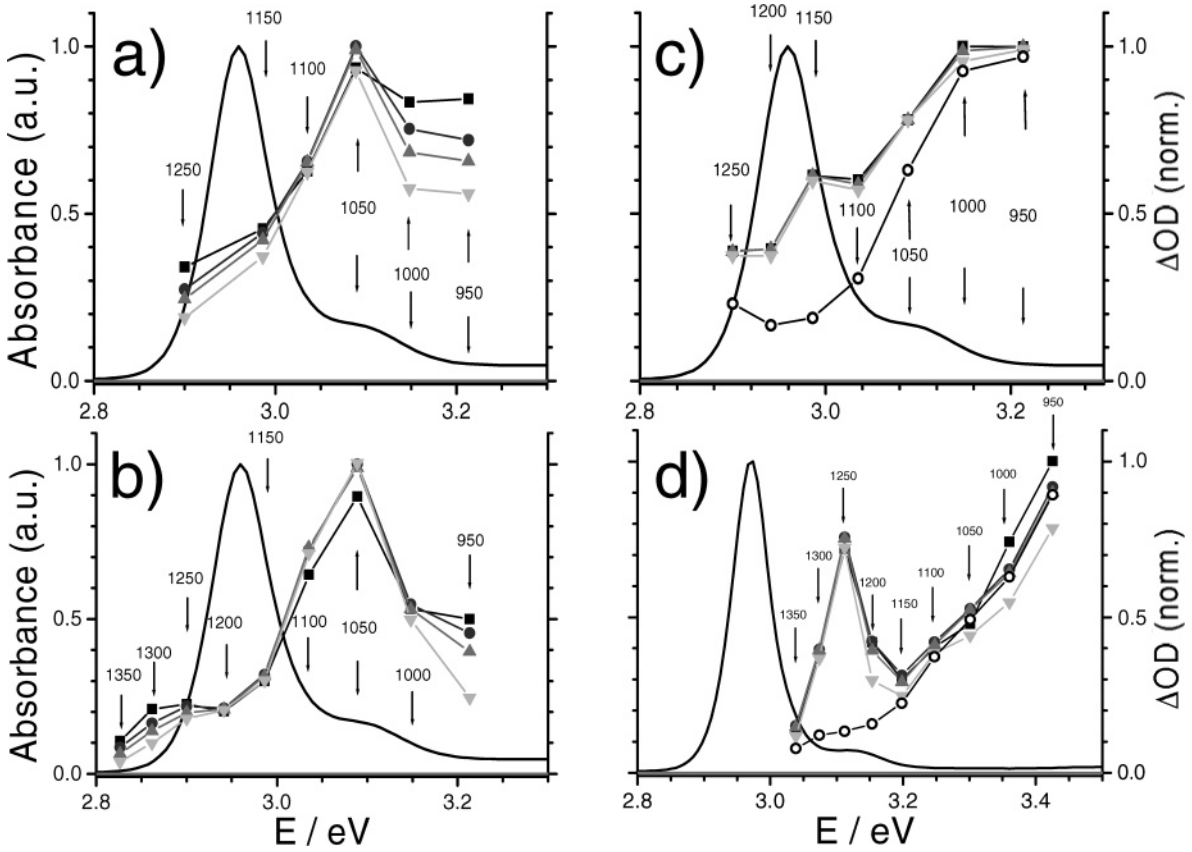

Figure 4. (a−c) Black line: Normalized steady-state spectrum of TTP−H_2 in the Soret region, the dotted lines are normalized transient spectra at pump wavelengths of 514, 546, and 647 nm for a, b, and c, respectively, after 200 fs (black squares), 500 fs (dark gray circles), 1 ps (gray triangles), and 20 ps (light gray reversed triangles). The probe wavelengths (in nm) are indicated. The energy assigned to the abscissa is the energy of the $Q_x(0,0)$ state (647 nm $\hat{=}$ 1.91 eV) of TTP−H_2 plus the probe pulse energy. (d) The same for ZnTTP with a pump wavelength of 546 nm and $Q(0,0)$ energy of 585 nm $\hat{=}$ 2.12 eV.

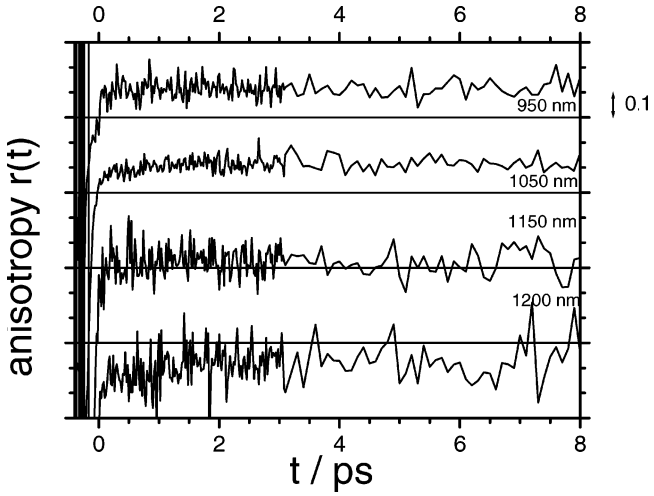

Figure 5. Transient anisotropy of TTP−H_2 after excitation with a 647 nm pulse for various probe wavelengths (shifted for clarity).

energy of the probe pulse. One recognizes a peak at 1250 nm and an increasing signal at wavelengths shorter than 1150 nm.

The anisotropy measurements are shown in Figure 9 for several probe wavelengths. A fast, wavelength independent component with $\tau_1^a = (150 \pm 30)$ fs is followed by a residual anisotropy r_s that does not decay within 100 ps. This residual anisotropy is 0.09 ± 0.01 for all wavelengths up to 1050 nm and increases to 0.13 for 950 nm. The significant difference between these curves are the time zero anisotropies r_0. For 1350 nm, $r_0 = -(0.18 \pm 0.03)$, at 1250 nm; that is, at the peak maximum, $r_0 = -(0.11 \pm 0.03)$. With decreasing wavelength, r_0 gradually increases up to 0.2 at 950 nm.

4. Discussion

4.1. Tetratolylporphyrin. The *Q* state dynamics of tetraphenylporphyrin (TPP−H_2) have been investigated intensively [34−36,71,72], either on a femtosecond-to-picosecond time scale[34−36] or nanosecond time scale.[71,72] Since the differences between a phenyl- and a tolyl-substituted porphyrin are small (the spectral shift is approximately 2 nm for TTP−H_2 and TPP−H_2 dissolved in benzene[74]), these results are considered to be valid also for TTP−H_2 (compare with Appendix B). In the femtosecond experiments described in the literature, the dynamics following excitation to the S_2 state (*B* band) were studied.[34−36] The probe wavelength in pump−probe experiments was always in the visible (the maximal probe wavelength being 702 nm[34]), thus probing higher (undefined) S states. At longer wavelength, even T_1 absorption could be detected.[34] In the present study, the minimal probe wavelength is 950 nm, larger than necessary for a $T_n \leftarrow T_1$ excitation ($\lambda_{T_2 \leftarrow T_1} < 850$ nm[75]); therefore, only singlet transitions have to be considered.

4.1.1. Excitation to the $Q_x(0,0)$ Band. Pump−Probe Experiments: Magic angle experiments with a pump wavelength of 650 nm (see Figure 3) show that excitation to the $Q_x(0,0)$ band does not lead to any relaxation within 100 ps in agreement with a Q_x lifetime of TPP−H_2 in benzene of 14 ns.[72] More interesting are the transient spectra and the anisotropy measurements (see Figure 4c and Figure 5). Compared with the Soret ground state excitation, the maximum is shifted some 0.22 eV toward the blue side. Note that the real value may

TABLE 1: Fit Parameters for TTP−H_2 after Excitation at 514 and 647 nm[a]

pump wavelength: 514 nm							
wavelength/nm	950	1000	1050	1100	1150	1200	1250
			transients				
τ_1/fs	190	180	180	140	80		150
τ_2/fs	1700	1200	900	2000	900		1700
$A_2 \times 10^{-3}$	0.42	0.61	0.37	0.17	0.25		0.22
$A_3 \times 10^{-3}$	1.59	1.62	2.65	1.75	1.10		0.56
$w(A_2)$/%	20.9	27.4	12.3	8.9	18.5		28.2
			anisotropy				
r_0	0.28	0.27	0.07	0	−0.02	−	−0.08
r_{max}	0.23	0.29	0.12	0.08	0.07		[b]
r_s	0.07	0.15	0.09	0.05	0.03		0.06
τ_1^a/fs	[c]	[d]	70	60	80		130
τ_2^a/fs	2300[c]	1900[d]	900	1200	1000		

pump wavelength: 650 nm							
wavelength/nm	950	1000	1050	1100	1150	1200	1250
			transients				
$A_1 \times 10^{-3}$	0.39	0.39	0.31	0.23	0.24	0.15	0.15
			anisotropy				
r_0		0.12	0.05	−0.02	−0.07	−0.18	−0.12
r_s	0.11	0.14	0.12	0.06	0.01	−0.08	−0.02
τ_1^a/fs		600	580	330	400	700	300

[a] The transients for 514 nm were fitted with a triexponential decay with time constants τ_1, τ_2, and τ_3[e] and amplitudes A_2 and A_3[f]. The relative weight $w(A_2)$ is defined in eq 2. The anisotropy is fitted with an exponential decay constant τ_1^a and a residual anisotropy r_s that did not change on a 10 ps time scale. A long time decay with a time constant of $\tau_l^a = (200 \pm 100)$ ps could be estimated from the measurements. r_0 denotes the time zero anisotropy. Since the transients for a pump wavelength of 650 nm do not show any dynamics, only the amplitude is given. [b] The profile does not provide a maximum. [c] The signal is not biexponential and exhibits a minimum and a maximum (see Figure 4). The value given for τ_2^a is a guess for the last time constant. [d] The profile is not biexponential. The value given for τ_2^a is a guess for the last time constant. [e] The time constants for τ_3 are omitted, because they exceed the time delay of the experiment. However, τ_3 decreases markedly with increasing probe wavelength. While it is beyond 1 ns for $\lambda_{probe} \leq 1000$ nm, it becomes ~350 ps for 1250 nm. [f] The amplitudes are taken from a biexponential fit. The value for A_2 represents the amplitude for the short time dynamics while the value for A_3 represents the long time dynamics.

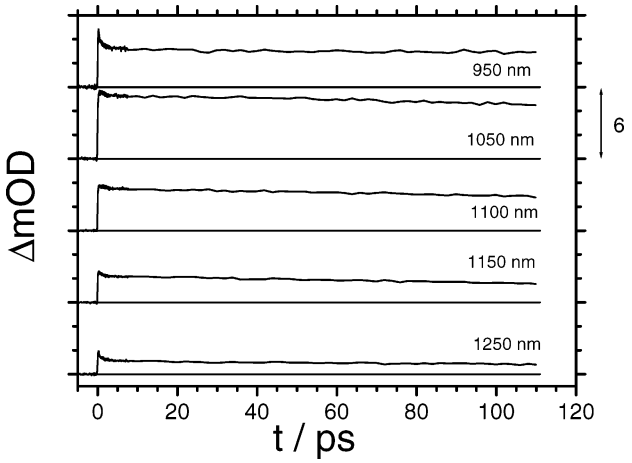

Figure 6. Transients of TTP−H_2 after excitation with 514 nm (shifed for clarity).

exceed 0.22 eV, since it is unclear whether the probe wavelength of 950 nm is short enough. The probed state may be assigned to a $1B_{2g}$ state. Although there are no calculations for TTP−H_2, nevertheless, the states and their related symmetries can be adapted from measurements of the free base porphyrin,[19,27−29] where the symmetry class is supposed to be D_{2h} (see Appendix B). The lowest gerade state is of B_{1g} symmetry and energetically in the vicinity of the Soret band (two bands of B_{2u} and B_{3u} symmetry) for all computational methods. A B_{2g} state can be found 0.6−0.8 eV above this state, that is, slightly lower than an A_g state. The value of the energy gap $E_{2B_{2/3u}} - E_{1B_{2g}}$ between the Soret maximum and the $1B_{2g}$ maximum could not be determined accurately by theoretical calculations, since the absorption spectrum shows a single absorption peak in the Soret region whereas theoretical calculations of free base porhyrin typically deliver an energy-splitting of the two Soret bands (with $2B_{2u}$ and $2B_{3u}$ symmetry) ranging between 0.03 eV using BP/ALDA[19] and 0.36 eV for SAC-CI[27] (see refs 28 and 29 for a comparison). The energy gap $\Delta E_{2B_{2/3u}-1B_{1g}}$ varies between 0 and 0.32 eV neglecting CIS and RPA calculations with 63-1+G(d) basis where the gap exceeds 0.7 eV.[28] Compared with these calculations, the experimental value of $\Delta E_{2B_{2/3u}-1B_{1g}} \geq 0.22$ eV is reasonable.

Anisotropy Measurements: As described in section 3.2.1 (see also Table 1), the time zero anistropy r_0 decreases with increasing probe wavelength. This behavior can only be understood, if (at least) two different states (further denoted as S_n and S_n', where $E(S_n) > E(S_n)'$) with nonparallel transition dipole moments ($\vec{\mu}_2$ for the transition $S_n \leftarrow Q_x$ and $\vec{\mu}_2'$ for the transition $S_n' \leftarrow Q_x$) are probed. Both states contribute partly to the anisotropy (as well as to the pump−probe response) with different amplitudes A_i^a. The highest anisotropy ($r_0 = 0.12$) is obtained at 1000 nm which correlates with the maximum of the transient spectra. The lowest anisotropy is at 1200 nm ($r_0 = -0.18$). Since a maximal ΔOD value was measured at 1150 nm, the transition is supposed to peak between 1150 and 1200 nm. Moreover, the S_n' state partly absorbs at 1050 nm, where the anisotropy starts to decrease. These two conditions are fulfilled by the Soret band. Intrinsically, two-photon excitation to the Soret band is electronically forbidden by selection rules assuming D_{2h} symmetry. Because of Jahn−Teller distortion, the transition should be weakly allowed (see appendix B). Since the Soret band is a transition with a large oscillator strength, one can expect that it also has a significant oscillator strength in a two photon process. In Figure 4c, a difference spectrum between the normalized transient spectrum (at 1 ps) and the

TABLE 2: Fit Parameters for TTP−H_2 after Excitation at 546 nm[a]

wavelength/nm	950	1000	1050	1100	1150	1200	1250	1300	1350
				transients					
τ_2/fs[b]	2500	1300	1200[c]	[d]	1400	620	710	700	690
$A_2 \times 10^{-3}$	0.40	0.28	0.008	0.003	0.01	0.06	0.29	0.47	0.32
$A_3 \times 10^{-3}$	0.50	1.89	5.28	2.77	1.14	0.78	0.68	0.41	0.17
$w(A_2)$/%	44.4	12.9	0.2	0.1	0.9	7.1	29.9	53.4	65.3
				anisotropy					
r_0	0.26	0.23	0.16	0.08	0.09	0.08	0.09	0.11	0.09
r_{max}						0.20	0.19	0.19	
r_s	0.18	0.19	0.11	0.13	0.10	0.18	0.17	0.14	0.13
τ_1^a/fs	510	380	210	340	300	210	130	130	200
τ_2^a/fs						210	500	500	

[a] The transients were fitted biexponentially with time constants τ_2 and τ_3 and amplitudes A_2 and A_3. The relative weight $w(A_2)$ is defined in eq 2. The anisotropy is fitted with an exponential decay constant τ_1^a and a residual anisotropy r_s that did not change on a 10 ps time scale. A long time decay with a time constant of $\tau_l^a = (200 \pm 100)$ ps could be estimated from the measurements. r_0 denotes the time zero anisotropy. [b] The time constants are denoted τ_2 and τ_3 rather than τ_1 and τ_1 in order to simplify the nomenclature in the discussion and comparison with the signals at a pump wavelength of 514 nm. The same is true for the amplitudes A_2 and A_3. [c] The signal is clearly triexponential and exhibits a rise with a time constant of $\tau_3 \approx 100$ ps. [d] The amplitude is too weak to give a reliable value of τ_2.

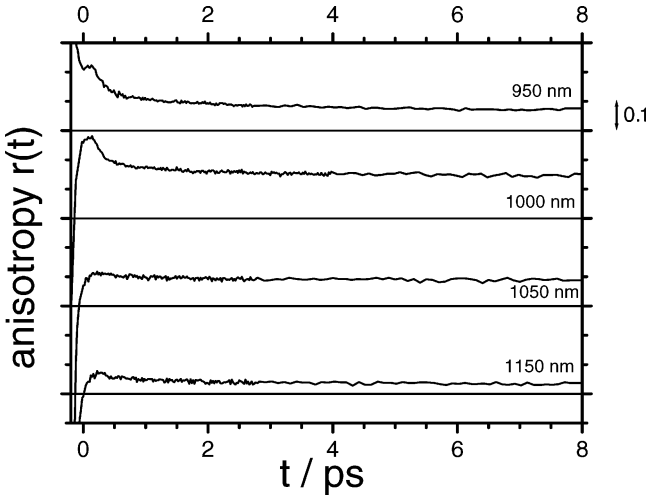

Figure 7. Transient anisotropy of TTP−H_2 after excitation with 514 nm (shifted for clarity).

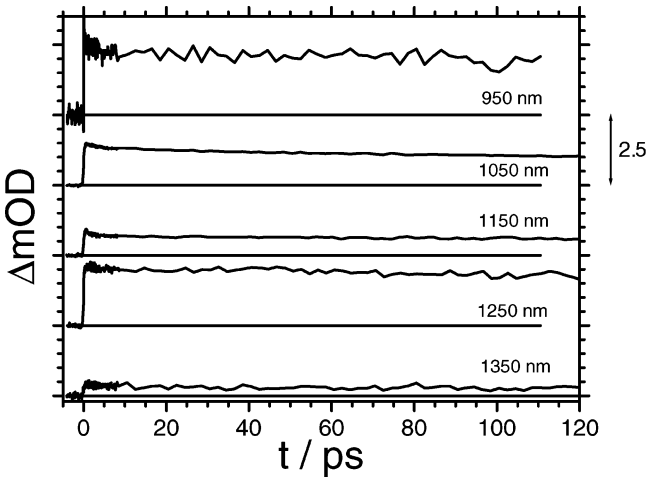

Figure 8. Transients of ZnTTP after excitation with 546 nm (shifted for clarity).

normalized Soret band is shown (open circles) exhibiting a maximum around 950 nm.

A third state may be recognized at 1250 nm: The difference spectrum is rising as does the anisotropy. Unfortunately, the transient response is weak because of the small oscillator strength of the $Q_x(0,0)$ band, so no additional probe wavelengths have been measured.

The time zero anisotropies r_0 are 0.10 ± 0.01 below the r_s value for $\lambda_{probe} \geq 1050$ nm, and the time constants vary between 330 and 700 fs. The anisotropy rise can be explained by the splitting of the Soret bands B_x and B_y. The dipole moments of these states are pointing toward the x and y directions of the porphyrin skeleton (see ref 12 for definition). Therefore, the $B_x(0,0) \leftarrow Q_x(0,0)$ and the $B_y(0,0) \leftarrow Q_x(0,0)$ transitions have different transition dipole moments leading to the conclusion that one transition is forbidden at time zero but is accessible after vibrational excitation of the molecule.[73] Usually, one would expect coherent vibrations; however, the temporal resolution of our setup and the low amplitude ratio are not good enough to observe these oscillations. Note that orientation relaxation cannot be a reason for the anisotropy decay, since the moments of inertia of TTP−H_2 ($I_1 = 1.865 \times 10^{-46}$ kg·m^2, $I_2 = 3.629 \times 10^{-46}$ kg·m^2, and $I_3 = 1.881 \times 10^{-46}$ kg·m^2 using DFT, B3LYP/SVP) and therewith the free correlation times $\tau_{c,i} = (2\pi/9)(I_i/k_BT)^{1/2}$ [76] ($\tau_{c,1} = 4.70$ ps, $\tau_{c,2} = 6.56$ ps, and $\tau_{c,3} = 4.72$ ps) are too large; furthermore, the anisotropy should decay to zero rather than to r_s.

In conclusion, excitation to the Q_x band reveals three states near the Soret region. The state with the lowest energy is probably the lowest gerade state (B_{1g}) as assigned by calculations. Additionally, the Soret band can also be reached because of the Jahn−Teller distortion. The state with the highest oscillator strength with a maximum at 3.20−3.25 eV is supposed to have B_{2g} symmetry.

4.1.2. Excitation to the Q_y Band. Pump−Probe Experiments: A more detailed picture of the relaxation pathways can be extracted from the transients when the molecule is pumped at 514 or 546 nm. These wavelengths deliver an excess energy of 0.5 and 0.36 eV, respectively, compared with the excitation to the $Q_x(0,0)$ band. Therefore, the higher lying $1B_{2g}$ and $1B_{3g}$ states can be reached (see Appendix B). The time constant(s) is(are) on the order of the time constants reported by Baskin et al. for TPP−H_2.[34] Thus, the $Q_y - Q_x$ transition occurs in < 200 fs and is even faster when exciting the $Q_y(0,0)$ transition. Vibrational relaxation occurs in about 1−2 ps. However, the analysis of τ_2 is quite complicated since several states can be probed by an NIR probe pulse as mentioned in 4.1.1. The time constant of 10−20 ps due to nonelastic scattering processes[34] are not seen in the presented experiments.

Inspection of the transient spectra of both pump wavelengths shows a maximum at 1050 nm (see Figure 4a,b), the spectra of $\lambda_{pump} = 546$ nm also exhibit a weak maximum at 1250 nm that

TABLE 3: Fit Parameters for ZnTTP after Excitation at 546 nm[a]

wavelength (nm)	950	1000	1050	1100	1150	1200	1250	1300	1350
					transients				
τ_1/fs	4900	4100	3200	1000	1200	1600	1700	3100	1500
$A_1 \times 10^{-3}$	0.48	0.32	0.12	0.07	0.13	0.23	0.04	0.02	0.06
$A_2 \times 10^{-3}$	2.08	1.50	0.64	0.54	0.35	0.42	1.53	0.53	0.17
$w(A_1)$/%	18.8	17.6	15.8	11.5	27.1	35.4	2.5	3.6	26.1
					anisotropy				
r_0	0.20	0.25	0.06	0.08	0.02	−0.04	−0.09	−0.14	−0.14
r_s/fs	0.13	0.19	0.10	0.05	0.08	0.09	0.09	0.08	0.09
τ_1^a/fs	150	160	180	120	60	140	160	110	140

[a] The transients were fitted biexponentially with time constants τ_1 and τ_2 (τ_2 was omitted since the time scale of the experiment was too short to draw any quantitative conclusions) and amplitudes A_1 and A_2. The relative weight $w(A_1)$ is defined in eq 2. The anisotropy is fitted with an exponential decay constant τ_1^a and a residual anisotropy r_s that did not change on a 10 ps time scale. r_0 denotes the time zero anisotropy.

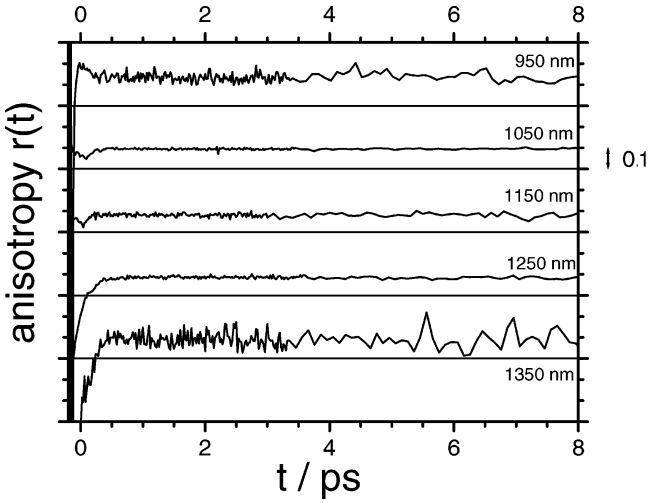

Figure 9. Transient anisotropy of ZnTTP after excitation with 546 nm (shifted for clarity).

decays on a picosecond time scale. Both spectra are similar despite the excess energy of 0.14 eV in the case of λ_{pump} = 514 nm. Therefore, a significant part of this energy must be deposited in vibrational modes that do not contribute to the probe process. Both sets of spectra must be compared with the spectra of λ_{pump} = 647 nm in Figure 4c. Remember that the energy on the abscissa is the sum of the energy of the Q_x state plus the probe wavelength. After 20 ps, the molecule is in the Q_x state but still vibrationally hot. Therefore, the spectra at λ_{pump} = 514 and 546 nm are blue-shifted compared with the spectrum of λ_{pump} = 650 nm at this delay time; that is, less energy is required to probe the same state. Consequently, the peak around 1050 nm is attributable to the B_{2g} state (see section 4.1.1) shifted by an excess energy of ~0.15 eV compared with spectra at λ_{pump} = 647 nm.

At λ_{pump} = 546 nm, the delayed rise of the transients at 1050 and 1100 nm might be interpreted as a spectral shift at early times. The small change of the ΔOD values at these wavelengths (i.e., the maximum of the transient spectra) and the more rapid decay on the spectral wings can be qualitatively understood with a model described in Appendix C. The time constants are nearly identical between 1000 and 1150 nm but distinctly smaller at 1200 nm (red edge). At 950 nm, the prolonged time constant indicates an influence of another transition. The fact that a picosecond dynamic of the transients at wavelengths >1250 nm can be seen shows that the relaxation process is not terminated after 500 fs. Moreover, one recognizes a decreasing time constant τ_3 with increasing probe wavelength as necessary for a red-edge transition. This analysis shows that at least one state is red-shifted with respect to the B_{2g} state, probably two when comparing with the spectra at λ_{pump} = 647 nm, namely, the Soret band and the B_{1g} state (see discussion of the anisotropy data below).

Anisotropy Measurements: The most relevant difference of the anisotropy data at various pump wavelengths are the different transition dipole moments of the Q_x and the Q_y bands, which are supposed to be perpendicular to each other. This may alter the anisotropy values significantly, but the time constants should be retained. For λ_{pump} = 546 nm, the transient anisotropy shows a biexponential decay for all wavelengths besides 950 nm. The different behavior at λ_{probe} = 950 nm is not surprising since this probe wavelength has already shown a different behavior in the pump−probe studies. At probe wavelengths assigned to the B_{2g} state (1000−1100 nm) after the initial Q_y−Q_x transition, the time zero anisotropy r_0 becomes smaller and remains constant for longer wavelengths. Probing the B_{2g} maximum at $E \geq 3.22$ eV, which is fullified by a combined energy of 546/1300 nm determines the r_0 value of the transition to the B_{2g} state. The higher values at shorter wavelengths ($E \geq 3.45$ eV) are due to a higher state (probably B_{3g}). For λ_{pump} = 514 nm, the time zero anisotropy is rising over the whole range probed. This can easily be understood as the combined energy 514 /1150 nm is 3.49 eV, thus being on the rising B_{3g} edge. The maximal anisotropy is reached between 950 and 1000 nm, that is, ~3.7 eV, which gives a clue for the position of this state.

The dynamics of the anisotropy are determined by a fast Q_y−Q_x transition. The decay (or rise) times of the anisotropy on a femtosecond time scale for the $Q_y(0,0)$ excitation for $\lambda_{probe} \leq 1100$ nm are faster but still comparable to the dynamics after $Q_x(0,0)$ excitation (200−400 instead of 350−700 fs). This effect can be explained as follows: The Q_y−Q_x transition is supposed to occur in ~100 fs according to the measurements of Baskin et al.[34] and as suggested by the pump−probe data (see above). This transition should be seen in the transient anisotropy as well. However, examination of the signals only shows (λ_{probe} = 1000 and 1050 nm) a single time constant instead of two (one for the Q_y−Q_x transition and one for the Soret splitting after vibrational motion; see preceding subsection). Note that the second time constant can be faster than the time resolution of the experiment. Assuming the existence of such a process and therewith a smaller time constant, τ_2 has to be larger than 200−400 fs, thus being in the range of the supposed *B*-band splitting as in the case of λ_{pump} = 647 nm. Further increase of the probe wavelength leads to a rise of r_s while the transient anisotropy exhibits a maximum at $t \approx 300$ fs, slightly depending on the wavelength. The existence of a maximum reveals that at least two different processes occur. After the Q_y−Q_x transition, the B_{2g} band is not (or only partly) accessible for these wavelengths, and the probe process leads to another band of gerade symmetry.

Therefore, the anisotropy rises to a value of r_{max}. The subsequent decay can only be explained if two bands overlap. According to section 4.1.1, these bands are the Soret and, at lower energy, the B_{1g} bands. The Soret band delivers a greater anisotropy; therefore, the anisotropy decreases after having passed the maximum. At 1350 nm, this band is not accessible anymore; so, the anisotropy rises without maximum.

The transient anisotropy for a pump wavelength of 514 nm also exhibits a maximum (except at a probe wavelength of 1250 nm), while the profiles are at least triexponential. One component termed τ_1^a can be assigned by a delayed Q_y-Q_x transition compared to an instantaneous $Q_y(0,0)$ excitation. The maximum can be explained by the superposition of two existing states. The $^1B_{2g}$ state has an excitation energy of ~3.2 eV as found by $Q_x(0,0)$ excitation (see section 4.1.1). In the course of the vibrational relaxation in the Q_x band, the oscillator strengths of the transitions to the $^1B_{2g}$ and the Soret states change. Since the $^1B_{2g}$ state is energetically higher, the $^1B_{2g} \leftarrow Q_x$ excitation results in a higher anisotropy compared with the B (Soret) $\leftarrow$ Q_x excitation. Therefore, the anisotropy gets smaller with increasing time and decreasing probe wavelength. At $\lambda_{probe} =$ 1250 nm, no maximum can be seen since the $^1B_{2g}$ state is not reached.

Concluding this section, the states found in the section 4.1.1 are also found when exciting the Q_y band. Additionally, a band with higher energy (B_{3g}) is found by inspecting the anisotropy data. Moreover, the excess energy delivered by pumping the Q_y band is partly distributed in vibrational modes that are not active for the excitation with the probe pulse.

4.2. Zinc-tetratolylporphyrin. Pump−Probe Experiments: TTP−H_2 and ZnTTP differ in their symmetries (D_{2h} compared with D_{4h}), resulting in a Q-band splitting of TTP−H_2 (Figure 1). The transient spectra shown in Figure 4d exhibit a maximum at 1250 nm (or 3.11 eV, when summing the energy of the vibrational ground state of the Q band and the probe pulse energy) and a rising edge at higher energies. This state cannot be the Soret band, since both the total energy is too high and the oscillator strength ought to be too large for a forbidden transition; therefore, it has to be a state of gerade symmetry, for example, the 1^1E_g state (see Appendix B). Due to the same symmetry of the Soret (1^1E_u) and the 1^1E_g bands (besides the parity), it is likely that both states exhibit a similar shape of the absorption band; therefore, the difference between the Soret band and the transient spectrum at 1 ps shifted by 0.14 eV is shown in Figure 4d (open circles; the construction is similar to Figure 4c). The remaining spectrum has a rising edge of at least one but probably two different strong gerade transitions (see discussion of the anisotropy).

The assignment of the time constants and the amplitudes follows the model described in Appendix C. The first time constant of $\tau_1 = (4.9 \pm 0.5)$ ps for $\lambda_{probe} = 950$ nm agrees well with the time constant of 5 ps for the vibrational cooling of the Q band of ZnTPP as measured by Yu et al.[33] At longer wavelengths (1000−1100 nm), the time constant decreases as required for vibrational cooling at the red edge of a single probe transition. Starting with 1150 nm, τ_1 slightly increases up to 1250 nm. At longer wavelengths, there exists no obvious trend. Additionally, the transients at 1100 and 1250 nm have a small amplitude A_1 for the τ_1 process. According to the analysis given above, there are (at least) two overlapping states that are responsible for the transient at 1100 nm (1^1E_g and 1^1A_{2g} and/or 1^1B_{2g}). The low ΔOD value indicates that a minimum between two maxima is probed. At 1250 nm, the maximum of the 1^1E_g band is reached. Besides the large ΔOD value, this is indicated again by a flat curve. The analysis of the amplitudes further allows the prediction, that the maximum of the transition is not reached with a probe wavelength of 950 nm. The large τ_1 value at 1300 nm can be explained by a shoulder or red-edge absorption of either the 1^1A_{2g} or the 1^1B_{2g} state, which may lie underneath the 1^1E_g band.

Anisotropy Measurements: Finally, the anisotropy measurements shall be discussed. There are three important features: (1) the decreasing time zero anisotropy with increasing probe wavelength, (2) the long time anisotropy, which is identical for $\lambda_{probe} \leq 1150$ nm and (3) the probe wavelength independent time constant of (150 ± 30) fs.

The identical value for r_s at $\lambda_{probe} \leq 1150$ nm is due to the same state that is probed for all wavelengths (see transient spectra in Figure 4d). At shorter wavelengths, eq 4 can be used to describe the increasing value. Excitation occurs no longer to the Soret band only but partly to a higher lying state. The smaller r_s anisotropy at $\lambda_{probe} = 950$ nm compared with $\lambda_{probe} \leq 1000$ nm is probably due to a second gerade state. According to the calculations, a possible assignment denotes the lower lying state with a maximum slightly red-shifted as the 1^1A_{2g} state and the band with a high oscillator strength as the 1^1B_{2g} band. Since the Soret band is shifted by 0.14 eV, the maximum of the 1^1A_{2g} band is at (3.25 ± 0.05) eV. Finally, τ_1^a can be explained by decoherence effects. It is known, that metallated porphyrins exhibit a degenerate Q band. In the case of MgTPP, this degeneracy can be seen by a degenerate pump−probe experiment at 620 nm, leading to an anomalous time zero anisotropy of 0.7 that decays biexponentially with time constants of (220 ± 13) fs and (4.9 ± 0.6) ps due to dephasing and population relaxation[55] (for a theoretical treatment, see ref 78 and references cited therein). In the experiments by Galli et al., only stimulated fluorescence was observed; in our case, higher lying states ("diffuse bands")[55] are probed; therefore, the time zero anisotropy is not 0.7. Nevertheless, τ_1^a can be assigned to the dephasing process of the Q band, since it is independent of the probe wavelength and therefore independent of the probed states (the effect of population relaxation is negligible).

4.3. Comparison with Previous Work. Previous investigations of dark states have only rarely been performed. Tobita et al. studied degenerate two photon excitations of ZnTPP at 540 nm, observing a gerade state of $^1A_{2g}$ symmetry.[60] The large oscillator strength in this region was comparable with the oscillator strength of the Soret band. A more systematic experimental analysis was executed by Rodriguez et al.,[79] who used femtosecond flash excitation at 582 nm and collected vis-NIR spectra after delays on a picosecond and a nanosecond time scale. Spectra were obtained for the $^1(\pi,\pi^*)$ and the $^3(\pi,\pi^*)$ states, respectively, of free base and metallated TPP and OEP (octaethylporphyrin) derivatives, that is, the spectra of the Q band and the ^{1}T state. They found a strong absorption peak on the red side of the Soret band but only a featureless structure in the region between 600 and 900 nm for the $^1(\pi,\pi^*)$ spectrum with a decaying absorption when increasing the wavelength toward the IR up to 1100 nm. A peak could only be found between 820 and 850 nm for the $^3(\pi,\pi^*)$ transitions of TPP derivatives. Similar spectra were found by Kubo et al. by exciting zinc pentafluoro-tetraphenyl-porphyrin (ZnFTPP) with a 15 ps pulse at 532 nm.[80] The strong absorption peak near the Soret band was explained by the excitation of a second electron instead of promoting an already excited electron to a higher state. The decaying absorption for ZnTPP in ref 79 up to 1100 nm is confirmed by the present study for ZnTTP; however, the additional peak at 1250 nm has not been previously observed.

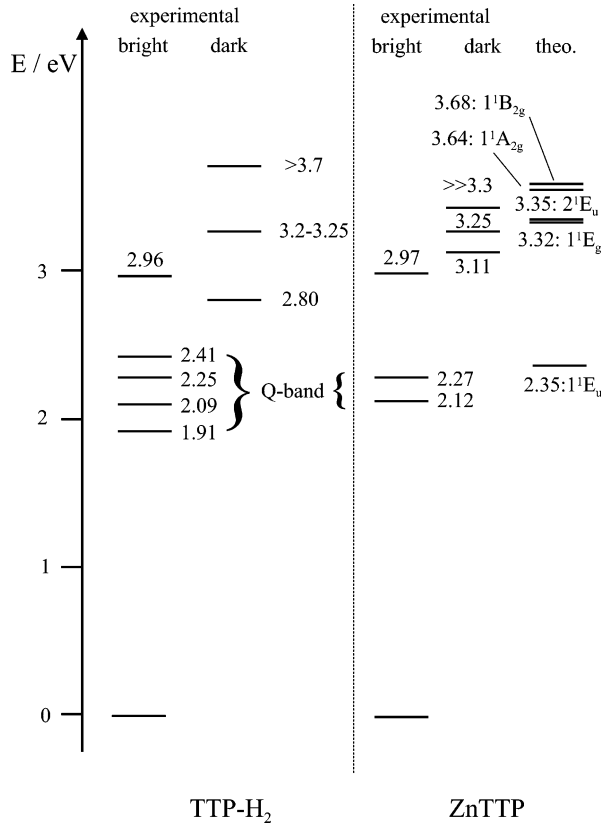

Figure 10. Energy level of electronic states of TTP−H_2 in CH_2Cl_2 and ZnTTP in cyclohexane. The bright states were obtained by UV−vis spectroscopy (Figure 1), and the dark states were obtained by analyzing the femtosecond measurements. The calculations are for ZnTPP by TDDFT(B3LYP/6-31G*) using a D_{4h} symmetry constraint.[30]

It cannot be explained by an excitation of a second electron, since the excitation energy of ~1 eV is too low. The same holds for TTP−H_2. The existence of such an excitation is crucial for the interpretation of femtosecond experiments with Soret band excitation, where bright or dark states in the vicinity of the Soret band are essential to explain for instance the diverse fluorescence decay and rise times of the *B* and *Q* bands, respectively,[30,33,34] since the relaxation processes for one- or two-electron excitations are clearly different.[60]

5. Conclusion and Outlook

We have presented the first visible pump/near-infrared probe femtosecond investigations of porphyrin systems, that is, free base tetratolylporphyrin in dichloromethane and zinc tetraphenylporphyrin in cyclohexane. Besides the study of the *Q* band dynamics of both systems, experimental evidence for the existence of the dark gerade states were obtained (see Figure 10 for an overview). The Soret band can be populated by a two photon process, but other states, especially at higher energies have a higher oscillator strength. In the case of TTP−H_2, the dark states lie at (2.80 ± 0.05) eV for the $1B_{1g}$ state, at 3.20−3.25 eV for the $1B_{2g}$ state, and at >3.7 eV for the $1B_{3g}$ state therefore, more red-shifted than predicted by the TDDFT-calculations. In the case of ZnTTP, the results are less clear. Besides the Soret band at 2.97 eV, there is one band at (3.11 ± 0.05) eV with ^1E_g symmetry, one at (3.25 ± 0.05) eV, probably of $^1A_{2g}$ symmetry, and one band at ≫3.30 eV, most likely of $^1B_{2g}$ symmetry. Our results give no evidence for a transition on the red side of the Soret band; however, after comparison with the measurements of TTP−H_2, such a transition could occur at lower energies than probed in the experiments, although no additional state is predicted by calculations.

At this point, two alternative interpretations shall also be discussed. First, the probed states might be vibrationally higher excited states of the Soret band, that do not have any oscillator strength in the one photon absorption spectrum. However, this cannot be the only explanation, since at least one transition is found beneath the excitation energy of the Soret transition. The second possibility is that there exists only one dark state with several vibronic states. This would contradict the quantum chemical calculations that predict several dark states. Moreover, the states are not equidistantly spaced as required for vibrational progression.

Further investigations may address this issue as well as the solvent dependence of the transients. Moreover, different systems like transition metal porphyrins may lead to a different dynamic. Finally, excitation of the remaining *Q* transitions of the porpyrins, for example, the $Q_x(1,0)$ transition of TTP, should give comparable results to the dynamics of the *Q*(1,0)-probe process of ZnTTP.

Acknowledgment. This work was partially supported by the Fonds der chemischen Industrie and by the Deutsche Forschungsgemeinschaft through the Karlsruhe Center of Functional Nanostructures (Project Nos. C3.2 and C3.5) at the University of Karlsruhe (TH).

Appendix A

Analysis of Anisotropy Signals. The transient anisotropy is calculated by eq 1. For a system with no degenerate states as it is the case for free base porphyrins, the anisotropy can be written as[66,67]

$$r(t) = \frac{1}{5}[3\langle \cos\beta(0)\cos\beta(t)\rangle - 1] \qquad (3)$$

where β denotes the angle between the transition dipole moment $\vec{\mu}_1$ of the pump and the transition dipole moment $\vec{\mu}_2$ of the probe transition. If several states participate in the pump or the probe processes, eq 3 can be written in a modified form as

$$r(t) = \frac{1}{5}\sum_{i=1}^{n} A_i^a(t)[3\langle \cos\beta_i(0)\cos\beta_i(t)\rangle - 1] \qquad (4)$$

where *i* reflects the different processes (i.e., transient bleaching, excited-state absorption or stimulated emission), β_i represents the angle between the corresponding transition dipole moments while A_i^a is the fraction of the process *i* ($\sum_i A_i^a = 1$). At $t = 0$, the so-called time zero anisotropy $r(0) = r_0$ only depends on the static position of the transition dipole moments. For $t > 0$, the anisotropy changes due to varying $A_i^a(t)$, rotational diffusion,[66] or decoherence effects.[78,81,82] Often these processes can be considered to behave exponentially.

Appendix B

Comparison of Quantumchemical Calculations. Calculations of free porphyrin have been performed by several groups using ab initio (RPA, DFT/B3LYP, SAC-CI, CAS-PT 2) as well as semiempirical methods (ZINDO).[19,27−29,83] The *Q* band energies are between 1.79 eV (RPA/6-311++G**) and 2.34 eV (DFT/B3LYP/6-311++G**) for the Q_x band ($1B_{3u}$ symmetry) and between 1.94 eV (RPA/6-311++G**) and 2.49 eV (DFT/B3LYP/6-311++G**) for the Q_y band ($1B_{2u}$ symmetry) compared with experimental values of 1.98 and 2.42 eV;[84] the

energies for the *B* bands ($2B_{2u}$ and $2B_{3u}$ symmetry) are between 3.43 eV (DFT/B3LYP/6-311++G**) and 4.06 eV (RPA/6-311++G**) with a difference of ~0.1 eV between the B_x and the B_y band. The experimental value is 3.33 eV. The higher states ($3B_{3u}$ and $3B_{2u}$) are underestimated by all methods (by 0.3 eV for DFT/B3LYP to 1.5 eV for RPA). Additionally, three bands with gerade symmetry can be found ($1B_{1g}$, $1B_{2g}$, and $1B_{3g}$). DFT/B3LYP calculations deliver 3.57, 4.10, and 4.17 eV[29] for these states, while other methods result in higher values. For DFT as well as SAC-CI and ZINDO calculations, the $1B_{1g}$ state is only 0.1−0.2 eV above the energy of the Soret band, while the other states are ≥0.7 eV. Comparison of the energies for different methods results in large differences. The results with the smallest deviation from the experimental values are DFT/B3LYP calculations, especially at higher energies. Therefore, the dark states of porphyrins are expected at values delivered by this method.

While there are no calculations for a phenyl or a tolyl derivate for the free base, ZnTPP has already been studied by TDDFT (B3LYP/6-31*) calculations. Assuming D_{4h} symmetry, excitation energies of 2.35 eV (1^1E_u), 3.35 (2^1E_u), and 3.73 (3^1E_u) could be found.[30] The gerade states are located at 3.32 eV (1^1E_g), 3.64 eV (1^1A_{2g}), and 3.68 eV (1^1B_{2g}).

Besides the deviations of the measurements themselves, one has to consider that the porphyrins do not have exactly D_{2h} or D_{4h} symmetry. Instead, the minimum of the potential energy surface can be found in C_{2v} symmetry due to a Jahn−Teller distortion;[30] however, since this distortion is not supposed to be relevant, the higher symmmetry is used throughout this publication.

Appendix C

Qualitative Visualization of the Temporal Evolution of the Pump−Probe Profiles. In order to interpret the time constants τ_1 and τ_2 and the amplitudes of the pump−probe experiments, consider a simplified model shown in Figure 11a,b. After excitation of TTP−H_2 in the Q_y band, an isoenergetic transition to the vibrationally hot Q_x band occurs. Intramolecular vibrational energy redistribution (IVR) and collisions with the surrounding solvent will cause the molecule to dissipate excess energy. The probe pulse with the highest pump photon energy $h\nu_1$ in Figure 11a (black) excites the molecule to the maximum of the absorption line of the S_n state. Hence, the oscillator strength of the $S_n \leftarrow Q_x$ transition does not vary significantly during the cooling process as does the ΔOD profiles (e.g., Figure 6 for 516/1050 nm). Next, consider the excitation at the red edge of the absorption maximum at $h\nu_2$ (gray). The ΔOD signal is weaker after the cooling process since the transition process has less oscillator strength. If the probe energy further decreases ($h\nu_3$, light gray color), the time constant for the vibrational relaxation will also decrease, since the slope of the transition (e.g., a Gaussian slope) is steeper than $\exp(-x)$[77] or in a more descriptive fashion: The excitation of the largest wavelength faces sparse oscillator strength earlier during the relaxation process than a shorter wavelength. Therefore, the obtained time constant seems to be faster. Now consider the case of two absorption levels S_n and S_n' as seen in Figure 11b. For simplicity, the oscillator strength of both levels is supposed to be identical. The excitation with the lowest energy (light gray) mainly excites the porphyrin to the higher lying S_n state as before. However, after vibrational relaxation, the excitation leads principally to the S_n' state. Therefore, the amplitude for the τ_1 process decreases and no clear behavior of the time constant can be predicted. When the probe wavelength is increased further, the blue edge of the S_n' transition will be probed. In this case, the effect is inverse compared with probing at the red edge: The time constant increases with increasing wavelength and the amplitude of the τ_1 process also increases. Please note, that the analysis of shoulders (as seen in the Soret band of porphyrins) complicates the analysis considerably.

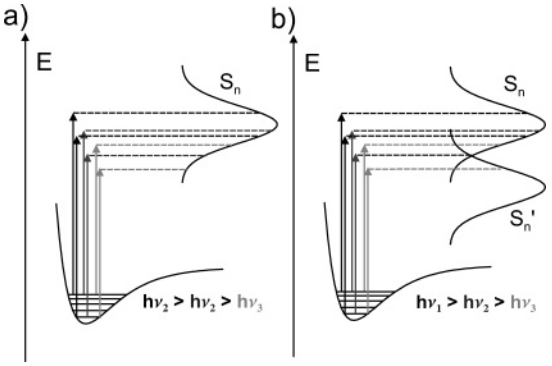

Figure 11. Qualitative visualization of the temporal evolution of the pump−probe profiles (see text for details).

References and Notes

(1) a) Dolphin, D., Ed. *The Porphyrins*; Academic Press: New York, 1978. b) Kadish, K. K.; Smith, K. M.; Guilard, R. *The Porphyrin Handbook*; Academic Press: San Diego, 2000.
(2) Kay, A.; Humphry-Baker, R.; Grätzel, M. *J. Phys. Chem.* **1994**, *98*, 952.
(3) Nazeeruddin, M. K.; Humphry-Baker, R.; Officer, D. L.; Campbell, W. M.; Burrell, A. K.; Grätzel, M. *Langmuir* **2004**, *20*, 6514.
(4) Wu, D.; Shen, Z.; Xue, Z. L.; You, M. *Chin. J. Inorg. Chem.* **2007**, *23*, 1.
(5) Yeow, E. K. L.; Steer, R. P. *Chem. Phys. Lett.* **2003**, *377*, 391.
(6) de Silva, A. P.; Leydet, Y.; Lincheneau, C.; McClenaghan, N. D. *J. Phys.: Condens. Matter* **2006**, *18*, S1847.
(7) Chen, X.; Drain, C. M. *Drug Design Rev.* **2004**, *1*, 215.
(8) Szaciłowski, K.; Macyk, W.; Drzewiecka-Matuszek, A.; Brindell, M.; Stochel, G. *Chem. Rev.* **2005**, *105*, 2647.
(9) Gottumukkala, V.; Luguya, R. J.; Fronczeck, F. R.; Vincente, M. G. H. *Bioorg. Med. Chem.* **2005**, *13*, 1633.
(10) Donzello, M. P.; Ercolani, C.; Stuzhin, P. A. *Coord. Chem. Rev.* **2006**, *250*, 1530.
(11) Wu, H.; Micca, P. L.; Makar, M. S.; Miura, *M. Bioorg. Med. Chem.* **2006**, *14*, 5083.
(12) Gouterman, M. In *The Porphyrins;* Dolphin, D., Ed.; Academic Press: New York, 1979; Vol. 3, p 1.
(13) Kalyanasundaram, K. *Photochemistry of Polypyridine and Porphyrin Complexes*; Academic Press: London, 1992.
(14) Tripathy, U.; Steer, R. P. *J. Porphyrins Phthalocyanines* **2007**, *11*, 228.
(15) Gouterman, M. *J. Mol. Spectrosc.* **1961**, *6*, 138.
(16) Gouterman, M.; Wagnière, G. H.; Snyder, L. C. *J. Mol. Spectrosc.* **1963**, *11*, 108.
(17) Serrano-Andrés, L.; Merchán, M.; Rubio, M.; Roos, B. O. *Chem. Phys. Lett.* **1998**, *295*, 195.
(18) Stratmann, R. E.; Scuseria, G. E.; Frisch, M. J. *J. Chem. Phys.* **1998**, *109*, 8218.
(19) van Gisbergen, S. J. A.; Rosa, A.; Ricciardi, G.; Baerends, E. J. *J. Chem. Phys.* **1999**, *111*, 2499.
(20) Sundholm, D. *Chem. Phys.* **2000**, *317*, 392.
(21) Baerends, E. J.; Ricciardi, G.; Rosa, A.; van Gisbergen, S. J. A. *Coord. Chem. Rev.* **2002**, *230*, 5.
(22) Rogers, J. E.; Nguyen, K. A.; Hufnagle, D. C.; McLean, D. G.; Su, W.; Gossett, K. M.; Burke, A. R.; Vinogradov, S. A.; Patcher, R.; Fleitz, P. A. *J. Phys. Chem. A* **2003**, *107*, 11331.
(23) Zhang, Y.-H.; Ruan, W.-J.; Li, Z.-Y.; Wu, Y.; Zheng, J.-Y. *Chem. Phys.* **2005**, *315*, 201.
(24) Tokura, S.; Tsuneda, T.; Hirao, K. *J. Theor. Comput. Chem.* **2006**, *5*, 925.
(25) Nakatsuji, H.; Hasegawa, J.; Hada, M. *J. Chem. Phys.* **1996**, *104*, 2321.
(26) Nooijen, M.; Bartlett, R. J. *J. Chem. Phys.* **1997**, *106*, 6449.
(27) Tokita, Y.; Hasegawa, J.; Nakatsuji, H. *J. Phys. Chem. A* **1998**, *102*, 1843.
(28) Šeda, J.; Burda, J. V.; Leszczynski, J. *J. Comput. Chem.* **2005**, *26*, 294.

(29) Šeda, J.; Burda, J. V.; Brázdová, V.; Kapsa, V. *Int. J. Mol. Sci.* **2004**, *5*, 196.
(30) Liu, X.; Yeow, E. K. L.; Velate, S.; Steer, R. P. *Phys. Chem. Chem. Phys.* **2006**, *8*, 1298.
(31) Karolczak, J.; Kowalska, D.; Lukaszewicz, A.; Maciejewski, A.; Steer, R. P. *J. Phys. Chem. A* **2004**, *108*, 4570.
(32) Lukaszewicz, A.; Karolczak, J.; Kowalska, D.; Maciejewski, A.; Ziolek, M.; Steer, R. P. *Chem. Phys.* **2007**, *331*, 359.
(33) Yu, H.-Z.; Baskin, J. S.; Zewail, A. H. *J. Phys. Chem. A* **2002**, *106*, 9845.
(34) Baskin, J. S.; Yu, H.-Z.; Zewail, A. H. *J. Phys. Chem. A* **2002**, *106*, 9837.
(35) Zhong, Q.; Wang, Z.; Liu, Y.; Zhu, Q. H.; Kong, F. *J. Chem. Phys.* **1996**, *105*, 5377.
(36) He, Y.; Xiong, Y.; Zhu, Q. H.; Kong, F. *Acta Phys. Chim. Sin.* **1999**, *15*, 636.
(37) Chosrowjan, H.; Tanigichi, S.; Okada, T.; Takagi, S.; Arai, T.; Tokumaru, K. *Chem. Phys. Lett.* **1995**, *242*, 644.
(38) Gurzadyan, G. G.; Tran-Thi, T.-H.; Gustavsson, T. *J. Chem. Phys.* **1998**, *108*, 385.
(39) Kumble, R.; Palese, S.; Lin, V. S.-Y.; Therien, M. J.; Hochstrasser, R. M. *J. Am. Chem. Soc.* **1998**, *120*, 11489.
(40) Yu, H. Z.; Baskin, J. S.; Steiger, B.; Wan, C. Z.; Anson, F. C.; Zewail, A. H. *Chem. Phys. Lett.* **1998**, *293*, 1.
(41) Akimoto, S.; Yamazaki, T.; Yamazaki, I.; Osuka, A. *Chem. Phys. Lett.* **1999**, *309*, 177.
(42) Cho, H. S.; Song, N. W.; Kim, Y. H.; Jeoung, S. C.; Hahn, S.; Kim, D. *J. Phys. Chem. A* **2000**, *104*, 3287.
(43) Mataga, N.; Shibata, Y.; Chosrowjan, H.; Yoshida, N.; Osuka, A. *J. Phys. Chem. B* **2000**, *104*, 4001.
(44) Kim, Y. H.; Jeong, D. H.; Kim, D.; Jeoung, S. C.; Cho, H. S.; Kim, S. K.; Aratani, N.; Osuka, A. *J. Am. Chem. Soc.* **2001**, *123*, 76.
(45) Kano, H.; Kobayashi, T. *J. Chem. Phys.* **2002**, *116*, 184.
(46) Min, C.-K.; Joo, T.; Yoon, M.-C.; Kim, C. M.; Hwang, Y. N.; Kim, D.; Aratani, N.; Yoshida, N.; Osuka, A. *J. Chem. Phys.* **2001**, *114*, 6750.
(47) Yatskou, M. M.; Koehorst, R. B. M.; van Hoek, A.; Donker, H.; Schaafsma, T. J.; Gobets, B.; van Stokkum, I.; van Grondelle, R. *J. Phys. Chem. A* **2001**, *105*, 11432.
(48) Hwang, I.-W.; Cho, H. S.; Yeong, D. H.; Kim, D.; Tsuda, A.; Nakamura, T.; Osuka, A.; *J. Phys. Chem. B* **2003**, *107*, 9977.
(49) Zamyatin, A. V.; Gusev, A. V.; Rodgers, M. A. J. *J. Am. Chem. Soc.* **2004**, *126*, 15436.
(50) Morandeira, A.; Vauthey, E.; Schuwey, A.; Gossauer, A. *J. Phys. Chem. A* **2004**, *108*, 5741.
(51) Fujitsuka, M.; Cho, D. W.; Shiragami, T.; Yasuda, M.; Majima, T. *J. Phys. Chem. B* **2006**, *110*, 9368.
(52) Cho, B. M.; Carlsson, C. F.; Jimenez, R. *J. Chem. Phys.* **2006**, *124*, 144905.
(53) Dietzek, B.; Maksimenka, R.; Kiefer, W.; Hermann, G.; Popp, J.; Schmitt, M. *Chem. Phys. Lett.* **2005**, *415*, 94.
(54) Luo, L.; Lo, C.-F.; Lin, C.-Y.; Chang, I.-J.; Diau, E. W.-G. *J. Phys. Chem. B* **2006**, *110*, 410.
(55) Galli, C.; Wynne, K.; LeCours, M.; Therien, M. J.; Hochstrasser, R. M. *Chem. Phys. Lett.* **1993**, *206*, 493.
(56) Schmitt, M.; Heid, M.; Schlücker, S.; Kiefer, W. *Biopolymers* **2002**, *67*, 226.
(57) Barbosa Neto, N. M.; Oliveira, S. L.; Misoguti, L.; Mendonça, C. R.; Gonçalves, P. J.; Borissevitch, I. E.; Dinelli, L. R.; Romualdo, L. L; Batista, A. A.; Zilio, S. C. *J. Appl. Phys.* **2006**, *99*, 123103.
(58) Moffitt, W. *J. Chem. Phys.* **1954**, *22*, 320.
(59) Moffitt, W. *J. Chem. Phys.* **1954**, *22*, 1820.
(60) Tobita, S.; Kaizu, Y.; Kobayashi, H.; Tanaka, I. *J. Chem. Phys.* **1984**, *81*, 2962.
(61) Tsuchiya, S. *J. Am. Chem. Soc.* **1999**, *121*, 48.
(62) Adler, A. D.; Longo, F. R.; Finarelli, J. D.; Goldmacher, J.; Assour, J.; Korsakoff, L. *J. Org. Chem.* **1967**, *32*, 476.
(63) Wilhelm, T.; Piel, J.; Riedle, E. *Opt. Lett.* **1997**, *22*, 1494.
(64) Riedle, E.; Beutter, M.; Lochbrunner, S.; Piel, J.; Schenkl, S.; Spörlein, S.; Zinth, W. *Appl. Phys. B* **2000**, *71*, 457.
(65) Gouterman, M.; Khalil, G.-E. *J. Mol. Spec.* **1974**, *53*, 88.
(66) Fleming, G. R. *Chemical applications of ultrafast spectroscopy;* Oxford University Press: Oxford, 1986.
(67) Kawski, A. *Crit. Rev. Anal. Chem.* **1993**, *23*, 459.
(68) Ferrer, M. L.; del Monte, F. *Langmuir* **2003**, *19*, 650.
(69) Kishii, N.; Shirai, K.; Tamura, S.-I.; Seto, J.; Tokumaru, K.; Takagi, S.; Arai, T.; Sakuragi, H. *J. Lumin.* **1995**, *64*, 125.
(70) Tokumaru, K. *J. Porphyrins Phthalocyanins* **2001**, *5*, 77.
(71) Gradyushko, A. T.; Tsvirko, M. P. *Opt. Spectrosc.* **1971**, *31*, 1.
(72) Ohno, O.; Kaizu, Y.; Kobayashi, H. *J. Chem. Phys.* **1985**, *82*, 1779.
(73) Another interpretation one might think of is the oscillation of the molecule around the Jahn-Teller active mode. This can lead to an effective (time averaged) planarization of the molecule corresponding to a D_{2h} symmetry. In this case, the Soret-excitation $B(0,0) \leftarrow Q_x(0,0)$ would be more strictly forbidden compared with the ground state leading to a higher anisotropy since the excitation occurs from the B_{2g} state. However, some dynamics for $\tau < 500$ ps should be seen in the pump−probe profiles.
(74) Moet-Ner, M.; Adler, A. D. *J. Am. Chem. Soc.* **1975**, *97*, 5107.
(75) Pekkarinen, L.; Linschitz, H. *J. Am. Chem. Soc.* **1960**, *82*, 2407.
(76) Bartoli, F. J.; Litovitz, T. A. *J. Chem. Phys.* **1972**, *56*, 413.
(77) Let us consider a relaxation process from a certain vibrational state to the ground state in an arbitrary time, e.g., 10 ps. Let the probe wavelength be λ_1. Assume further that, after these 10 ps, the signal has decreased by a facor of 1/2. If the slope of the excited state would be $\exp(-x)$, the signal would also decrease by a factor of 1/2 during 10 ps for every $\lambda_2 < \lambda_1$ (neglecting vibrational progression and Franck-Condon factors, but since the porphyrin skeleton is rather rigid, these processes can be neglected in a first approximation).
(78) Qian, W.; Jonas, D. M. *J. Chem. Phys.* **2003**, *119*, 1611.
(79) Rodriguez, J.; Kirmaier, C.; Holten, D. *J. Am. Chem. Soc.* **1989**, *111*, 6500.
(80) Kubo, M.; Mori, Y.; Otani, M.; Murakami, M.; Ishibashi, Y.; Yasuda, M.; Hosomizu, K.; Miyasaka, H.; Imahori, H.; Nakashima, S. *J. Phys. Chem. A* **2007**, *111*, 5136.
(81) Wynne, K.; Hochstrasser, R. M. *Chem. Phys.* **1993**, *171*, 179.
(82) Wynne, K.; Hochstrasser, R. M. *J. Raman Spectrosc.* **1995**, *26*, 561.
(83) Loboda, O.; Tunell, I.; Minaev, B.; Ågren, H. *Chem. Phys.* **2005**, *312*, 299.
(84) Edwards, L.; Dolphin, D. H.; Gouterman, M.; Adler, A. D. *J. Mol. Spectrosc.* **1971**, *38*, 16.